Transgenic mouse models in migraine

Ven, R.C.G. van de

SEVEN

CHAPTER 7

T_1 relaxation in *in vivo* mouse brain at ultra-high field

R.C.G. van de Ven,[1#] B. Hogers,[2#] A.M.J.M. van den Maagdenberg,[1,3] H.J.M. de Groot,[4] M.D. Ferrari,[3] R.R. Frants,[1] R.E. Poelmann,[2] L. van der Weerd,[2] S.R. Kiihne[4]

[#]Authors contributed equally

Department of [1]Human Genetics, [2]Anatomy & Embryology and [3]Neurology, Leiden University Medical Center, Leiden, The Netherlands.
[4]Leiden Institute of Chemistry, Leiden University, Leiden, The Netherlands.

Magnetic Resonance in Medicine, 58 (2007) p. 390-395.

Abstract

Accurate knowledge of relaxation times is imperative for adjustment of MRI parameters to obtain optimal signal-to-noise ratio and contrast. As small animal MRI studies are extended to increasingly higher magnetic fields, these parameters must be assessed anew. The goal of this study was to obtain accurate spin-lattice (T_1) relaxation times for the normal mouse brain at field strengths of 9.4 and 17.6 T. T_1 relaxation times were determined for cortex, corpus callosum, caudate putamen, hippocampus, periaqueductal gray, lateral ventricle and cerebellum and varied from 1651 to 2449 ms at 9.4 T and 1824 to 2772 ms at 17.6 T. Our findings are compared to literature T_1 values of both human and murine brain at different field strengths. A field strength-dependent increase of T_1 relaxation times is shown. The signal-to-noise ratio increase at 17.6T is in good agreement with expected SNR increase for a sample-dominated noise regime.

Abbreviations

MRI, magnetic resonance imaging; NMR, nuclear magnetic resonance; ROI, region of interest; T, Tesla; TE, echo time; TR, repetition time; SNR, singnal-to-noise ratio.

Introduction

Increasing knowledge of the mouse nervous system and the availability of a large number of transgenic models have made the mouse a very popular species to study neurological disorders. Non-invasive imaging techniques, such as MRI, have shown great potential to study brain pathology in these models.[1,2] However, the small size of the mouse brain has considerable implications for obtaining a spatial resolution comparable to that routinely obtained with MRI in patients; the small voxel size used in mouse brain imaging results in a very low signal-to-noise ratio (SNR) at normal, medical field strengths ($\leq$ 3 T). Therefore, increasingly high magnetic field strengths (up to 17.6 T) are used to increase the SNR.[3] Higher field strengths may also have positive effects on contrast-to-noise, e.g. for the BOLD effect used in functional MRI, MRS and magnetization transfer experiments.[4,5]

The application of higher field requires adjustment of image acquisition parameters, which are based on knowledge of the NMR tissue properties. Here, we focus on the spin-lattice relaxation time T_1, which can be used to assess neuropathology, such as tumors, multiple sclerosis, cerebral edema and infarction.[6] T_1-weighted imaging is also used extensively for contrast-enhanced MRI and to assess blood-brain-barrier integrity and perform molecular imaging.[7] The field dependence of T_1 may give considerable insight into the molecular origins of this image contrast mechanism, which will be useful in understanding how T_1 is related to disease processes.

Reports on T_1 relaxation times for mouse brain are limited mainly to systems of up to 11.7 T.[8-10] Relaxation data of mouse brain at 17.6 T are lacking completely. In this study we aim at validating quantitative T_1 imaging at high fields using phantoms. In addition, we provide the first *in vivo* T_1 relaxation maps of mouse brain at 17.6 T and compare those with measurements at 9.4 T. The results are discussed in terms of field dependence of the *in vivo* T_1 relaxation times and SNR.

Methods

Phantoms

Phantom tubes were prepared by diluting a stock solution of 0.5 M Gd-DOTA (Dotarem, Guerbet Nederland BV, Gorinchem, the Netherlands) in phosphate buffered saline. To produce a range of T_1 values the following dilutions were used: 1:5.000; 1:10.000; 1:25.000; 1:100.000 and 1:200.000. The T_1 relaxation times were determined by both MRI and high-resolution NMR at field strengths of 9.4 and 17.6 T.

Mice

In vivo imaging was performed on 6 female C57BL/6Jico mice aged 3 months (Charles River, Maastricht, the Netherlands). Before imaging, mice were initially anesthetized with 4% isoflurane in air (0.3 l min^{-1}) and O_2 (0.3 l min^{-1}) and maintained with ~1.5% isoflurane during all procedures. The respiratory rate was monitored via an air-pressure cushion connected to a laptop using Biotrig software (Bruker, Rheinstetten, Germany). The depth of the anesthesia was continuously regulated to maintain a stable respiration rate during each experiment. The body temperature of the animals was kept constant by pumping warm water through the gradient system, resulting in a constant temperature of the animal bed of 26°C. All animal experiments were performed in accordance with the guidelines of the Leiden University and national legislation.

MRI

Imaging was performed on two vertical 89-mm-bore magnets (Bruker BioSpin, Rheinstetten, Germany) with field strengths of 9.4 T (400 MHz) and 17.6 T (750 MHz). A Bruker Mini0.5 gradient system of 200 mT/m and a transmit/receive birdcage radiofrequency coil with an inner diameter of 38 mm was used on both systems. Bruker ParaVision 3.0 software was used for image acquisition.

A multiple spin echo saturation recovery method was used with variable repetition time (TR). Slice excitation and refocusing were accomplished by three-lobed sinc pulses with matched bandwidths, resulting in 90° and 180° pulse lengths of 1.0 and 0.81 ms, respectively. Imaging parameters were: echo time (TE) = 3.5 ms; 8 echoes; TR-array at 9.4 T = 0.1, 0.12, 0.15, 0.3, 0.5, 0.9, 1.5, 3, 6, 12 and 20 s; TR-array at 17.6 T = 0.1, 0.12, 0.15, 0.3, 0.5, 0.9, 1.5, 3, 6, 10 and 30 s; matrix = 128 x 128; FOV = 25.6 mm; slice thickness = 1 mm. All images were acquired as single slices to avoid interslice modulation effects and unwanted stimulated echoes were suppressed by spoiler gradients in the slice direction. The slice was positioned through the center of all phantom tubes or dorsally through the middle of the cerebellum and rostrally through the olfactory bulb.

Although 8 echoes were acquired to determine T_2 relaxation times, the T_2 values for the phantoms obtained at 17.6 T were extremely sensitive to processing parameters, did not show the expected T_2 dependence upon Gd-DOTA concentration, and were shorter than the high-resolution NMR values by 50% or more. For these reasons, quantitative localized T_2 measurements were not pursued *in vivo*.

High-resolution NMR

To validate the relaxation time measurements, relaxation rates in the phantoms were obtained by both MRI and high-resolution NMR. To keep experimental conditions as

equal as possible, the same phantoms and magnets were used and experiments were performed on the same day. Radiation damping was avoided in the high-resolution experiments by using a restricted sample volume in untuned, low Q probes at both field strengths. A broadband 5-mm solution-state NMR probe with a 120-µl sample tube was used at 9.4 T, while a triple-tuned magic angle spinning probe with a 400-µl sample holder was used at 17.6 T.

T_1 was measured using an inversion recovery spin echo experiment. The 90° and 180° pulse lengths were 25 and 50 µs, respectively. We used a variable list of eleven inversion times that were changed appropriately to the expected T_1 of each sample. Both TR and the longest inversion time were kept at > 10 x the expected T_1 of the sample.

Relaxation Analysis by MRI

Phase correction was performed on the entire complex data matrix using the linear zero- and first-order phase procedure in Bruker Paravision 3.0.

Regions of interest (ROIs) were defined bilaterally for each individual mouse in cortex, corpus callosum, caudate putamen, hippocampus, periaqueductal gray, lateral ventricle and cerebellum. The relaxation curves were phased to avoid baseline artefacts and the real part was used for the relaxation fits.[11] For the T_1 fits, eleven TR values with a fixed TE of 7 ms (second echo) were used. The T_1 values of the various ROIs were determined using a three-parameter saturation recovery fit function:

$$M(t) = \mathrm{A} + M_0(1 - \exp(-t/T_1)) \qquad [1]$$

where M_0 is the equilibrium magnetization. All fits were performed using a non-linear least square algorithm provided by the Image Sequence Analysis (ISA) tool of ParaVision 3.02. T_1 maps were generated on a pixel-by-pixel basis with the ISA tool.

Relaxation Analysis by High-Resolution NMR

Spectra were line-broadened (10 Hz Lorentzian) and Fourier transformed. The zeroth order phase was adjusted on the time point with the highest SNR and the same phase parameters were applied to all spectra in the experiment. Maximal intensities were detected automatically and fitted to a three-parameter inversion recovery equation:

$$M(t) = M_0(1 - 2\alpha\exp(-t/T_1)) \qquad [2]$$

where α is the inversion angle.

Signal-to-noise

SNR was calculated by placing a ROI in the tissue of interest and comparing the mean signal intensity (*SI*) with the standard deviation (SD) of the noise obtained from a large

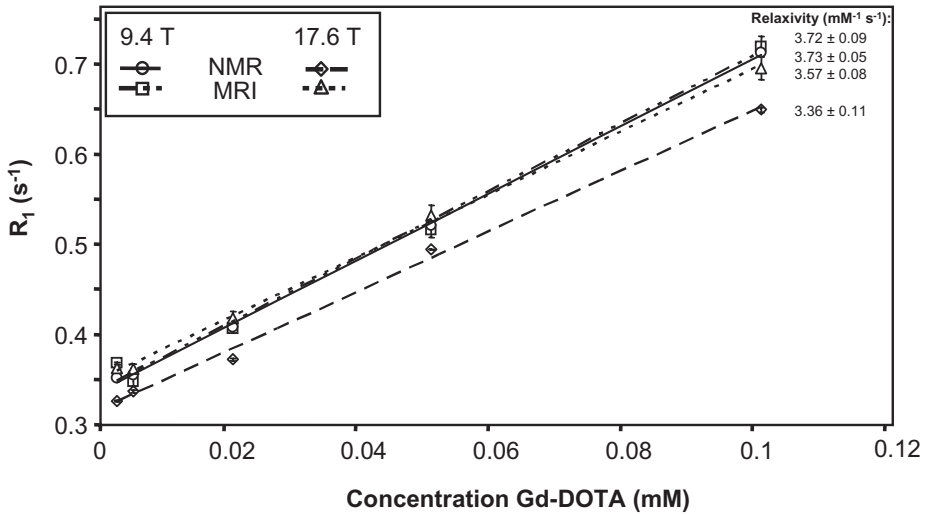

Figure 1. Relaxation measurements of phantoms using imaging and high-resolution NMR. R_1 relaxation rates as a function of Gd-DOTA concentration yields relaxivity. Mean R_1 in s^{-1} ± error bars (SD). Relaxivity in $nM^{-1}\ s^{-1}$ ± SD.

ROI placed in the image background, outside the mouse, $\mathrm{SNR} = \frac{SI}{\mathrm{SD}_{\mathrm{noise}}}$

Statistics

T_1 times at 9.4 and 17.6 T were compared by two-way repeated measures ANOVA. T_1 times of the different ROIs were compared by averaging the results of the left and right hemisphere for each individual animal, after which an unpaired two-tailed Student's t-test with Bonferroni-Holmes correction for multiple comparisons was done. Statistical analyses were performed using SPSS software (version 11, Chicago, IL). Data is presented as mean ± standard deviation.

Table 1 In vivo T_1 relaxation times of mouse brain at 9.4 and 17.6 T

	CC	Cor	H	PAG	CPu	V	CerG	CerW
9.4 T	1750 ± 45	1886 ± 122	1821 ± 47	1700 ± 65	1746 ± 31	2449 ± 150	1814 ± 118	1651 ± 28
17.6 T	1832 ± 86	2027 ± 106	1901 ± 77	1842 ± 108	1824 ± 101	2772 ± 235	2038 ± 63	1888 ± 112
Factor increase	1.05	1.07	1.04	1.08	1.04	1.13	1.12	1.14

Mean relaxation times in ms ± SD. CC, corpus callosum; CerG; cerebellum gray matter; CerW, cerebellum white matter; Cor, cortex; CPu, caudate putamen; H, hippocampus; PAG, periaqueductal gray; V, ventricle.

Results

Phantoms

Gd-DOTA phantoms of various concentrations were prepared to validate the MRI protocol for T_1 measurements against a standard inversion recovery high-resolution NMR protocol. At 9.4 T no significant differences were found between the MRI results and the high-resolution NMR results (Fig. 1). At 17.6 T the imaging method yielded T_1 values that were consistently 10% shorter than for the high-resolution NMR method. Despite these differences, a plot of R_1 versus the Gd-DOTA concentration yields straight lines with similar slopes for the two methods (Fig. 1). The Gd-DOTA relaxivities determined from the slopes are also given in Figure 1. At 9.4 T, the Gd-DOTA relaxivity was about 10% higher than the manufacturer's value at 1.5 T of 3.4 $mM^{-1} s^{-1}$; at 17.6 T the relaxivity was decreased by about 9% compared to 9.4 T.

Mice

T_1 relaxation times were determined *in vivo* at 9.4 and 17.6 T. ROIs were selected in cortex, corpus callosum, caudate putamen, hippocampus, periaqueductal gray, lateral ventricle and cerebellum (Fig. 2a). Table 1 summarizes the T_1 relaxation times calculated from these ROIs. Within this study, T_1 times significantly increase with field strength (two-way repeated measures ANOVA, $p = 0.018$). Additionally, T_1 maps were generated on a pixel-by-pixel basis (Fig. 2b, c).

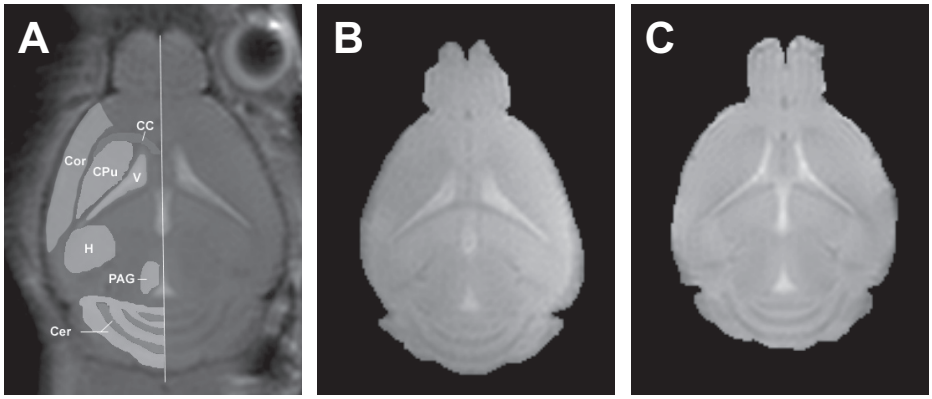

Figure 2. ROIs selected in a single T_2-weighted spin echo image (**A**). CC, corpus callosum; Cer, cerebellum; Cor, cortex; CPu, caudate putamen; H, hippocampus; PAG, periaqueductal gray; V, lateral ventricle. T_1 maps at 9.4 T (**B**) and 17.6 T (**C**) are depicted. The images are calculated from mono-exponential fits to 11 saturation recovery images with TE of 7 ms and TRs ranging from 100 ms to 20000 ms at 9.4 T or 30000 ms at 17.6 T.

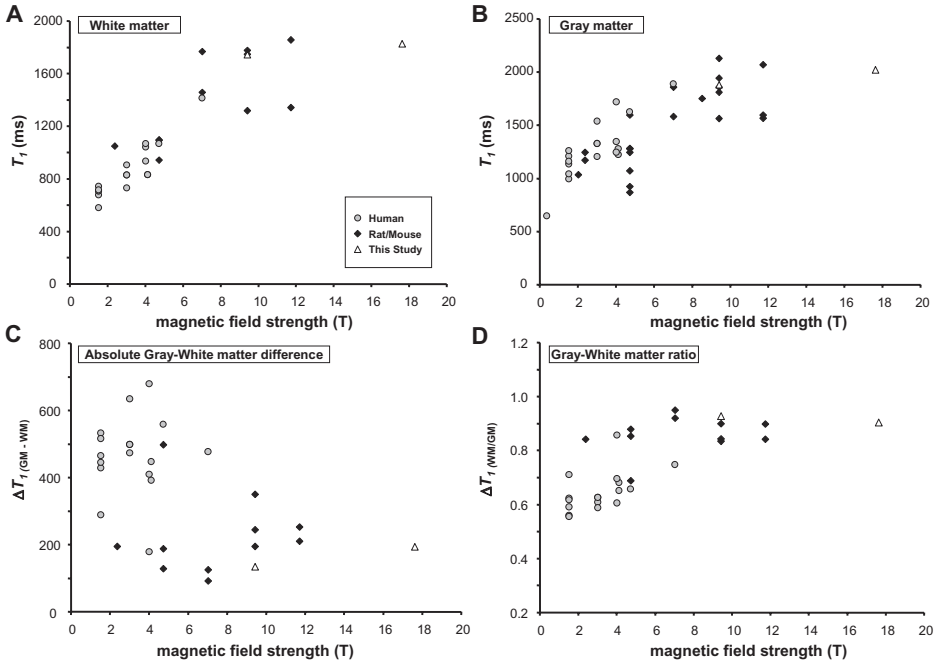

Figure 3. Magnetic field dependence of T_1. White (**A**) and gray (**B**) matter T_1 values in rodent (mouse and rat, black diamonds) and human (gray circles) brain are plotted based on literature data (refs. 8-10,12-37) and the experimental data from this study (white triangles). Absolute gray-white matter differences were calculated by subtraction of gray and white matter T_1 values of the same study (**C**). Relative gray-white matter ratios were calculated by dividing white and gray matter T_1 values of the same study (**D**).

We also performed a literature study to compare T_1 relaxation in rodent[8-10,12-23] and human[24-37] brain for different field strengths (Fig. 3). Our data tie in well with previous data on rodent gray and white matter. Due to limited datapoints per field strength, the variation in protocols between the literature sources and the theoretical non-linearity of field dependent T_1 increase, it is not informative to perform statistical analysis on the data presented in Fig 3a and b. Nonetheless, there clearly is a positive trend towards increasing T_1 times - for both gray and white matter in both rodents and humans - with field strength. Based on Fig. 3c and d, there is no statistical evidence that either the absolute or the relative difference in T_1 between gray and white matter changes with increasing field strength. Interestingly, the gray and white matter difference in T_1 is significantly larger in humans ($p = 0.0001$).

Signal-to-noise

The SNR performance of both imaging field strengths was compared for the mouse data. For all mice, the SNR was calculated using a ROI in the cortex on the second echo in every spin echo data set (proton density-weighted image; TE = 7 ms and TR = 20 or 30 s). The average experimental increase in SNR between 9.4 T and 17.6 T was 1.95 ± 0.09. This increase may be slightly underestimated because of a decrease in T_2 at higher field. Nonetheless, these values are in good agreement with expected SNR increase for a sample-dominated noise regime (SNR $\propto B_0 = 17.6/9.4 = 1.87$).

Discussion and Conclusions

Relaxation Times

Here we report T_1 relaxation times of mouse brain at both 9.4 and 17.6 T. These results are obtained on the same mice using consistent protocols, allowing direct comparison of measurements. The *in vivo* T_1 relaxation times are obtained for specific mouse brain regions, allowing comparison with other studies at different field strengths. These data can be used for optimization of high field imaging protocols. They also provide baseline values for relaxation times obtained in pathology in (transgenic) mice.

Published NMR relaxation values in rodent and human brain are scarce. We summarized available data in Fig. 3. This figure clearly shows the large variation in the reported values, which is caused by different hardware, pulse sequences and protocols, mouse and rat strains, age, fitting procedures etc. In our measurements, care was taken to avoid most of the mentioned constraints in order to obtain the fairest comparison possible between the different magnetic field strengths. In particular, we note that careful phasing and the use of real data are required to minimize baseline effects and obtain quantitative agreement with high-resolution NMR methods.[11] Despite the variability in T_1 values, it is obvious that T_1 increases with increasing field strength for both rodent and human brain, and that this trend continues up to 17.6 T. In studies with matched protocols at different field strengths, always a significant increase of T_1 was found with field strength (e.g. this study, refs[30,37]). Interestingly, the difference in gray matter T_1 and white matter T_1 is larger in humans than in rodents at every field strength. This may be due to differences in cytoarchitecture between the species, with humans e.g. having a lower neuron density.[38] Also, the rodent measurement were all performed under anaesthetics, which are known to change tissue perfusion[39] and can thereby affect the T_1 measurements, particularly in the gray matter.

Signal-to-noise

The use of high magnetic field results in increased SNR. Some advantages are that shorter acquisition times may be used and spatial resolution increased. The observed SNR increase at higher field depends on field strength and on the sample size and properties relative to the coil size. For very small samples, coil noise predominates resulting in a field dependence of SNR $\propto B_0^{7/4}$.[40] For large conductive samples, such as living mice, the sample noise dominates over coil noise, in particular at high magnetic fields and large sample diameter. Under these limiting conditions the noise increases linearly with resonance frequency and thus SNR $\propto B_0$.[41] The SNR increase in images of mouse brain was 1.95, which is in good agreement with expected SNR increase for a sample-dominated noise regime (SNR $\propto B_0 = 17.6/9.4 = 1.87$).

Field Dependence

An understanding of relaxation processes at the molecular level can provide a link between image intensity and tissue viability or biological processes. It is well known that the observed water T_1 relaxation in tissues is dominated by the much shorter T_1 relaxation of protons on macromolecules that are in contact with exchanging water molecules.[42,43] Relaxation theory predicts that T_1 increases with increasing field strength and eventually reaches a plateau at the solvent T_1. The T_1 of water is practically flat over the full range of NMR accessible measurements (except for the small effects of dissolved paramagnetic oxygen). At 17.6T, we measured a T_1 of tap water of 3.3 s, which is significantly longer than the observed tissue T_1. The continuing T_1 difference indicates that the local magnetic field of the *in vivo* water protons is modulated at high frequencies, enabling relatively efficient relaxation when compared to the solvent.

In conclusion, we have determined regional T_1 values of mouse brain *in vivo* at 9.4 and 17.6 T for future reference. The results show that T_1 still increases with field strength at ultra-high magnetic fields. The large gain in SNR encourages the use of ultra-high fields and merits further work in this direction.

Acknowledgements

The authors acknowledge Fons Lefeber and Kees Erkelens for technical assistance. This work was supported by a grant of the Netherlands Organization for Scientific Research (NWO) (Vici 918.56.602, M.D.F), the EU "EUROHEAD" grant (LSHM-CT-2004-504837; M.D.F, R.R.F, A.M.J.M.v.d.M) and the Centre for Medical Systems Biology (CMSB) established by the Netherlands Genomics Initiative/Netherlands Organization for Scientific Research (NGI/NWO).

References

1. Choi,I.Y., Lee,S.P., Guilfoyle,D.N. & Helpern,J.A. In vivo NMR studies of neurodegenerative diseases in transgenic and rodent models. *Neurochem. Res.* **28**, 987-1001 (2003).
2. Van der Weerd,L., Thomas,D.L., Thornton,J.S. & Lythgoe,M.F. MRI of animal models of brain disease. *Methods Enzymol.* **386**, 149-177 (2004).
3. Hu,X. & Norris,D.G. Advances in high-field magnetic resonance imaging. *Annu. Rev. Biomed. Eng* **6**, 157-184 (2004).
4. Benveniste,H. & Blackband,S. MR microscopy and high resolution small animal MRI: applications in neuroscience research. *Prog. Neurobiol.* **67**, 393-420 (2002).
5. Hennig,J., Speck,O., Koch,M.A. & Weiller,C. Functional magnetic resonance imaging: a review of methodological aspects and clinical applications. *J Magn Reson. Imaging* **18**, 1-15 (2003).
6. Tofts,P.S. Quantitive MRI of the brain. Tofts,P.S. (ed.), pp. 111-142 (John Wiley and Sons, Chichester,2003).
7. Dijkhuizen,R.M. & Nicolay,K. Magnetic resonance imaging in experimental models of brain disorders. *J Cereb. Blood Flow Metab* **23**, 1383-1402 (2003).
8. Guilfoyle,D.N., Dyakin,V.V., O'Shea,J., Pell,G.S. & Helpern,J.A. Quantitative measurements of proton spin-lattice (T1) and spin-spin (T2) relaxation times in the mouse brain at 7.0 T. *Magn Reson. Med.* **49**, 576-580 (2003).
9. Kuo,Y.T., Herlihy,A.H., So,P.W., Bhakoo,K.K. & Bell,J.D. In vivo measurements of T1 relaxation times in mouse brain associated with different modes of systemic administration of manganese chloride. *J Magn Reson. Imaging* **21**, 334-339 (2005).
10. Lee,J.H., Silva,A.C., Merkle,H. & Koretsky,A.P. Manganese-enhanced magnetic resonance imaging of mouse brain after systemic administration of MnCl2: dose-dependent and temporal evolution of T1 contrast. *Magn Reson. Med.* **53**, 640-648 (2005).
11. Van der Weerd,L., Vergeldt,F.J., De Jager,A.J. & Van As,H. Evaluation of algorithms for analysis of NMR relaxation decay curves. *Magn Reson. Imaging* **18**, 1151-1158 (2000).
12. Calamante,F. *et al.* Early changes in water diffusion, perfusion, T1, and T2 during focal cerebral ischemia in the rat studied at 8.5 T. *Magn Reson. Med.* **41**, 479-485 (1999).
13. De Graaf,R.A. *et al.* High magnetic field water and metabolite proton T1 and T2 relaxation in rat brain in vivo. *Magn Reson Med* **56**, 386-394 (2006).
14. Eis,M., Els,T. & Hoehn-Berlage,M. High resolution quantitative relaxation and diffusion MRI of three different experimental brain tumors in rat. *Magn Reson. Med.* **34**, 835-844 (1995).
15. Hoehn-Berlage,M., Eis,M., Back,T., Kohno,K. & Yamashita,K. Changes of relaxation times (T1, T2) and apparent diffusion coefficient after permanent middle cerebral artery occlusion in the rat: temporal evolution, regional extent, and comparison with histology. *Magn Reson. Med.* **34**, 824-834 (1995).
16. Massicotte,E.M., Buist,R. & Del Bigio,M.R. Altered diffusion and perfusion in hydrocephalic rat brain: a magnetic resonance imaging analysis. *J Neurosurg.* **92**, 442-447 (2000).
17. Rajan,S.S. *et al.* MRI characterization of 9L-glioma in rat brain at 4.7 Tesla. *Magn Reson. Imaging* **8**, 185-190 (1990).
18. Schwarcz,A., Berente,Z., Osz,E. & Doczi,T. In vivo water quantification in mouse brain at 9.4 Tesla in a vasogenic edema model. *Magn Reson. Med.* **46**, 1246-1249 (2001).
19. Schwarcz,A., Berente,Z., Osz,E. & Doczi,T. Fast in vivo water quantification in rat brain oedema based on T(1) measurement at high magnetic field. *Acta Neurochir. (Wien.)* **144**, 811-815 (2002).
20. Ting,Y.L. & Bendel,P. Thin-section MR imaging of rat brain at 4.7 T. *J Magn Reson. Imaging* **2**, 393-399 (1992).
21. Van der Weerd,L. *et al.* Neuroprotective effects of HSP70 overexpression after cerebral ischaemia--an MRI study. *Exp. Neurol.* **195**, 257-266 (2005).
22. Van Dorsten,F.A. *et al.* Dynamic changes of ADC, perfusion, and NMR relaxation parameters in transient focal ischemia of rat brain. *Magn Reson. Med.* **47**, 97-104 (2002).
23. Zaharchuk,G. *et al.* Neuronal nitric oxide synthase mutant mice show smaller infarcts and attenuated apparent diffusion coefficient changes in the peri-infarct zone during focal cerebral ischemia. *Magn Reson. Med.* **37**, 170-175 (1997).

24. Barfuss,H., Fischer,H., Hentschel,D., Ladebeck,R. & Vetter,J. Whole-body MR imaging and spectroscopy with a 4-T system. *Radiology* **169**, 811-816 (1988).
25. Breger,R.K., Rimm,A.A., Fischer,M.E., Papke,R.A. & Haughton,V.M. T1 and T2 measurements on a 1.5-T commercial MR imager. *Radiology* **171**, 273-276 (1989).
26. Fan,G., Wu,Z., Pan,S. & Guo,Q. Quantitative study of MR T1 and T2 relaxation times and 1HMRS in gray matter of normal adult brain. *Chin Med J (Engl.)* **116**, 400-404 (2003).
27. Jezzard,P., Duewell,S. & Balaban,R.S. MR relaxation times in human brain: measurement at 4 T. *Radiology* **199**, 773-779 (1996).
28. Kim,S.G., Hu,X. & Ugurbil,K. Accurate T1 determination from inversion recovery images: application to human brain at 4 Tesla. *Magn Reson Med* **31**, 445-449 (1994).
29. Kwag,J.H. *et al.* Fast mapping of T1 relaxation times in the human brain gray and white matters at 7 Tesla. *Proc Intl Soc Mag Reson Med* **9**, 1346 (2001).
30. Lu,H. *et al.* Routine clinical brain MRI sequences for use at 3.0 Tesla. *J Magn Reson Imaging* **22**, 13-22 (2005).
31. Mason,G.F., Chu,W.J. & Hetherington,H.P. A general approach to error estimation and optimized experiment design, applied to multislice imaging of T1 in human brain at 4.1 T. *J Magn Reson* **126**, 18-29 (1997).
32. Schmitt,P. *et al.* Inversion recovery TrueFISP: quantification of T(1), T(2), and spin density. *Magn Reson Med* **51**, 661-667 (2004).
33. Takaya,N., Watanabe,H. & Mitsumori,F. Elongated T1 values in human brain and the optimization of MDEFT measurements at 4.7T. *Proc Intl Soc Mag Reson Med* 2339 (2004).
34. Van Walderveen,M.A., Van Schijndel,R.A., Pouwels,P.J., Polman,C.H. & Barkhof,F. Multislice T1 relaxation time measurements in the brain using IR-EPI: reproducibility, normal values, and histogram analysis in patients with multiple sclerosis. *J Magn Reson Imaging* **18**, 656-664 (2003).
35. Vrenken,H. *et al.* Whole-brain T1 mapping in multiple sclerosis: global changes of normal-appearing gray and white matter. *Radiology* **240**, 811-820 (2006).
36. Wansapura,J.P., Holland,S.K., Dunn,R.S. & Ball Jr.,W.S. NMR relaxation times in the human brain at 3.0 tesla. *J Magn Reson Imaging* **9**, 531-538 (1999).
37. Weigel,M. & Hennig,J. Contrast behavior and relaxation effects of conventional and hyperecho-turbo spin echo sequences at 1.5 and 3 T. *Magn Reson Med* **55**, 826-835 (2006).
38. DeFelipe,J., Alonso-Nanclares,L. & Arellano,J.I. Microstructure of the neocortex: comparative aspects. *J Neurocytol.* **31**, 299-316 (2002).
39. Stullken,E.H., Milde,J.H., Michenfelder,J.D. & Tinker,J.H. The nonlinear responses of cerebral metabolism to low concentrations of halothane, enflurane, isoflurane, and thiopental. *Anesthesiology* **46**, 28-34 (1977).
40. Mansfield,P. & Morris,P.G. NMR imaging in biomedicine. Waugh,J.S. (ed.) (Academic Press, New York,1982).
41. Edelstein,W.A., Glover,G.H., Hardy,C.J. & Redington,R.W. The intrinsic signal-to-noise ratio in NMR imaging. *Magn Reson. Med.* **3**, 604-618 (1986).
42. Bryant,R.G. The dynamics of water-protein interactions. *Annu. Rev. Biophys. Biomol. Struct.* **25**, 29-53 (1996).
43. Koenig,S.H., Brown III,R.D., Adams,D., Emerson,D. & Harrison,C.G. Magnetic field dependence of 1/T1 of protons in tissue. *Invest Radiol.* **19**, 76-81 (1984).